A Stochastic Precipitation Generator Conditioned by a Climate Index

ALEJANDRA DE VERA AND RAFAEL TERRA

Instituto de Mecánica de los Fluidos e Ingeniería Ambiental, Facultad de Ingeniería, Universidad de la República, Montevideo, Uruguay

(Manuscript received 23 October 2017, in final form 15 June 2018)

ABSTRACT

This work presents a stochastic daily precipitation generator that incorporates a climate index to reflect the associated, seasonally varying, influence on simulated precipitation statistics. The weather generator is based on a first-order, two-state Markov chain to simulate the occurrence of daily precipitation and a gamma distribution to compute the nonzero daily precipitation amounts. Therefore, it has four parameters that are, in turn, allowed to vary daily following an autoregressive linear model in Gaussian space that simulates the parameters' deviations from their climatological seasonal cycle. This model is forced by the independently predicted evolution of a climate index and captures how the model parameters and, therefore, precipitation are gradually shifted by the associated climate signal. In this case, the Niño-3.4 index is used to account for the influence of the El Niño–Southern Oscillation (ENSO) phenomenon on precipitation in Uruguay. However, the methodology is general and could be readily transferable to indices of other climate modes or downscaling algorithms for seasonal climate prediction. The results show that the proposed methodology successfully captures the ENSO signal on precipitation, including its seasonality. In doing so, it greatly reduces the underestimation of the seasonal and interannual precipitation variability, a well-known limitation of standard weather generators termed the ''overdispersion'' phenomenon. This work opens interesting opportunities for the application of seasonal climate forecasts in several process-based models (e.g., crop, hydrological, electric power system, water resources), which may be used to inform the decision-making and planning processes to manage climate-related risks.

1. Introduction

Stochastic weather generators (WGs) have been widely used in decision support systems for risk-based planning and management of natural resources, linked to different process models (e.g., crop, hydrological and electric power system). The proper management of these resources requires a suitable representation of the risks associated with climate variability at different temporal and spatial scales. Particularly, due to the advances in global circulation models (GCMs) and seasonal climate predictions, during the last few decades there has been a growing interest in the use of weather generators as downscaling tools. This application poses additional requirements on weather generators, other than the basic ones of capturing seasonally varying weather statistics. They should be able to incorporate climate forecast information and simulate conditioned synthetic sequences that account for the forecast shift.

According to Brissette et al. (2007), stochastic weather generators can be divided into three main categories: parametric [based on the Weather Generator (WGEN) model; Richardson 1981; Wilks 1998], semiparametric/empirical [the best known is the Long Ashton Research Station Weather Generator (LARSWG); Semenov and Barrow 1997], and nonparametric (generally based on resampling methods; e.g., Rajagopalan and Lall 1999). We adopt the parametric approach, which has the advantage of being readily able to incorporate climate forecast information through appropriate adjustments to the model parameters (Wilks 2010). A comprehensive review of weather generators can be found in Wilks and Wilby (1999), Baigorria and Jones (2010), and Ailliot et al. (2015).

Several approaches have been proposed for the incorporation of climate forecast information into weather generators. One approach is to estimate the parameters of the model conditional to a given climate index that affects the local climate. Grondona et al. (2000) developed a stochastic precipitation generator conditioned on the

Corresponding author: Alejandra De Vera, adevera@fing.edu.uy

DOI: 10.1175/JAMC-D-17-0307.1

El Niño–Southern Oscillation (ENSO) phase with a range of parameterization schemes, in which the model parameters are estimated separately for warm and cold ENSO events, as well as neutral years. The approach was tested in six locations in east-central Argentina and western Uruguay (southeastern South America), an important agricultural region with a clear ENSO precipitation signal (Grimm et al. 2000). Wilby et al. (2002) explored the combination of several predictor variables in order to downscale both the high- and low-frequency components of daily precipitation at sites across the British Isles. Three daily precipitation models were considered: unconditional of low-frequency forcing, implicitly conditioned by daily airflow indices, and explicitly conditioned by mixtures of daily airflow indices and either the North Atlantic Oscillation (NAO) index or area-average sea surface temperature (SST) anomalies. An alternative approach starts from preexisting aggregated climatic variables (e.g., at monthly time scale) and then proceed to disaggregate or temporally downscale to daily frequency. Hansen and Ines (2005) implemented a stochastic weather generator that disaggregates monthly rainfall data by conditioning input parameters on forecast rainfall amounts or their predictors (e.g., ENSO phases) or by constraining the generated daily sequences to match the target rainfall totals. They demonstrate its use linked to a maize crop simulation model at three locations: two in the southeast United States and one in Kenya. More recently, Verdin et al. (2018) presented a parametric stochastic weather generator able to simulate sequences conditioned on interannual and multidecadal trends. The generalized linear modeling (GLM) framework of their weather generator allows any number of covariates to be included, such as large-scale climate indices, local climate information, seasonal precipitation, and temperature forecasts, among others. They applied this methodology to the Argentine Pampas. In conjunction with the GLM weather generator, Kim et al. (2016) used a resampling scheme to translate the uncertainty in the seasonal forecasts into the corresponding uncertainty for the daily weather statistics. They also extended this approach to the case of climate change scenarios.

The objective of the present study is to develop a stochastic daily precipitation generator that smoothly incorporates a climate index to reflect associated seasonally varying shifts in simulated precipitation statistics. To this end, we propose a modification of the standard stochastic weather generator Markov+Gamma (referred to as the base model), in which its parameters can gradually vary associated with a climate index. In this case, we use the Niño-3.4 index to account for ENSO phenomena. However, the methodology based on the ''analog days'' technique is general and could be readily transferable to other climate indices and downscaling algorithms. Results are shown for the Artigas weather station, located in the northern part of Uruguay (Fig. 1), where the ENSO signal is most significant. However, it could be readily implemented in any region featuring seasonal predictability associated with a climate mode or captured by an index derived from a downscaling scheme. Moreover, it could be applied in a multisite model following Wilks (1998), where simultaneous simulations at multiple locations are achieved with a collection of individual models fed by temporally independent but spatially correlated random numbers.

The paper is organized as follows. Rainfall data and ENSO influence on precipitation are presented in section 2. Section 3 contains a brief description and evaluation of the base model and in section 4 we introduce the modified methodology or ''proposed model.'' In section 5 we discuss the results. Finally, the conclusions are presented in section 6.

2. Local precipitation data and ENSO

a. *Rain gauge database*

We used daily precipitation data from 22 weather stations in Uruguay, between 1981 and 2015, provided by Instituto Uruguayo de Meteorología (InUMet) and Instituto Nacional de Investigación Agropecuaria (INIA). Weather station locations are indicated in Fig. 1, together with the mean annual precipitation (circle radius) that ranges between 1100 mm in the southwest and 1500 mm in the northeast for the 29-yr period (1981–2009) common to all 22 stations.

b. *ENSO influence on precipitation*

It is well known that the major single source of climate variability on seasonal-to-interannual scales in many parts of the world, including southeastern South America, is ENSO (Aceituno 1992), and that its influence presents a marked seasonality (Ropelewski and Halpert 1987, 1989; Díaz et al. 1998; Grimm et al. 2000; Cazes-Boezio et al. 2003).

During warm events or El Niño years, precipitation in Uruguay tends to be higher in certain seasons, especially from November to the following January and, although weaker, between March and July of the following year. Conversely, during cold events or La Niña years, precipitation tends to be below normal in similar periods. Even within Uruguay, there are regional variations in ENSO influence (Pisciottano et al. 1994; Montecinos et al. 2000).

To represent the climatic information associated with ENSO, we use the Niño-3.4 monthly index (referred to as N3.4; Trenberth 1997) between 1981 and 2015.

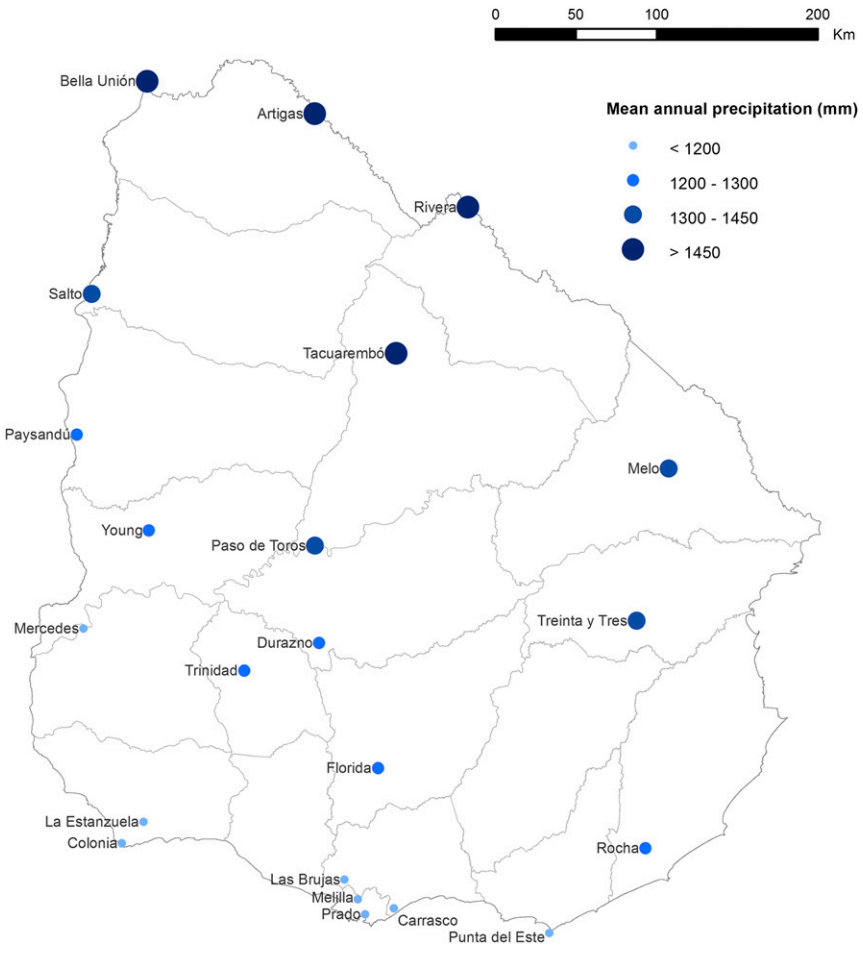

FIG. 1. Weather station locations. Circle radius denotes the mean annual precipitation for the 1981–2009 period.

This dataset consists of the area-average sea surface temperature anomalies over a region in the central equatorial Pacific Ocean (5°N–5°S, 120°–170°W) and is available online (www.cpc.ncep.noaa.gov/data/indices/sstoi.indices).

The proposed methodology (see section 4) requires a daily time series of a climatic index. We thus need to construct a daily N3.4 series for which there are several alternatives:

1) N3.4-NDJ: each day adopts the value of N3.4 averaged in the quarter November–January (NDJ) associated with the September–August ENSO year it falls in. Considering that NDJ is the peak season of the ENSO cycle, this methodology has been widely used to tag analog years in association with ENSO phenomena.
2) N3.4-Simultaneous: each day adopts the N3.4 value of the month it falls in. A 30-day moving filter may be applied to smooth the time series.
3) N3.4-OL: for each day of the year, a computation determines the lead time at which the index most conditions the precipitation [as in Maciel et al. (2015)] and assigns the associated value of N3.4.

In sections 4 and 5, we show the results using alternative 1 so that they can be readily compared with previous work using analog years. However, very similar results (not shown) were obtained using alternative 2.

Next, we present a quantification of the influence of ENSO (as represented by N3.4-NDJ) on local precipitation. Figure 2 shows the Pearson correlation maps between N3.4-NDJ and accumulated precipitation during September–August (ENSO year) and NDJ (season with strongest signal). We include the threshold of statistical significance at the 95% level according to a two-sided Student's t test (0.37). The correlation values increase from southeast to northwest, reaching values over 0.65 (0.60) for the NDJ (September–August) season, with statistically significant values in the northern half of the country approximately.

In addition, we analyzed the seasonal variation of ENSO's impact on a few rainfall-based statistics.

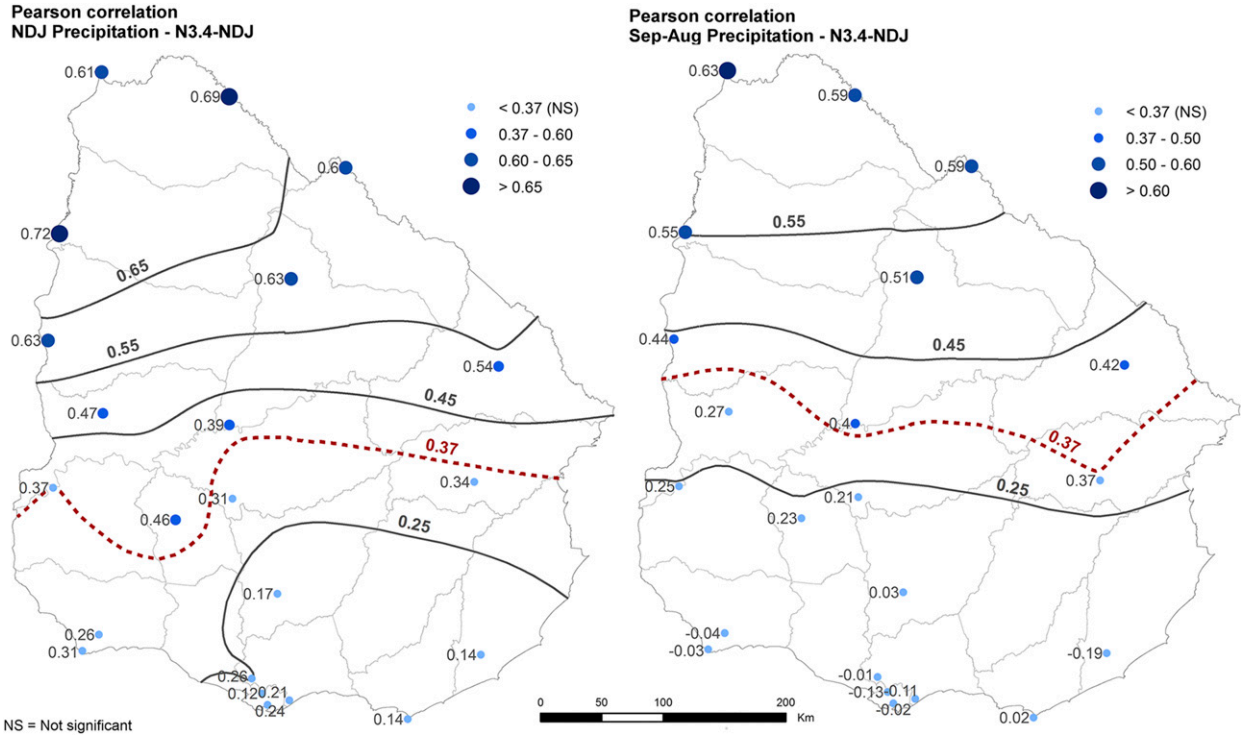

FIG. 2. Pearson correlation map between N3.4-NDJ and the (right) September–August and (left) NDJ accumulated precipitation for the 1981–2009 period. Statistical significance at the 95% level according to a two-sided Student's *t* test is indicated.

We classified each September–August year according to the N3.4-NDJ index and divided the results into quartiles. The first quartile (Q1) roughly corresponds to La Niña years (cold events) and the top quartile (Q4) is associated with El Niño years (warm events). Results are shown for the Artigas weather station (30.40°S, 56.50°W) located in the northern part of Uruguay, where the ENSO signal is most significant. The data series includes the daily total amount of rainfall for a 35-yr period from 1981 to 2015, a few years longer that the common record for all stations.

Figure 3 shows the annual cycle of daily precipitation (with centered moving windows of ±30 days) for all years and for Q1 and Q4 ensembles. Statistical significance was assessed through a Monte Carlo method. One thousand random samples of 8 years (same length as Q1 and Q4) were drawn out of all years and the 5th and 95th quantiles of the 8-yr average are indicated for each day. Periods for which Q1 or Q4 ensembles fall below or above those quantiles are shaded as significant to the 95% level. As expected, precipitation is above (below) average during Q4 (Q1) years, most significantly during spring and early summer. Moreover, the ENSO signal is somehow stronger during Q4 (El Niño events) than during Q1 (La Niña events).

Figures 4 and 5 present equivalent results for two "weather within climate" statistics: the probability of a given day falling into a heavy rainfall event and a dry spell, respectively. A "strong rainfall event" is considered to occur when the precipitation accumulated over 3 days exceeds 50 mm. Figure 4 shows that the probability of a given day falling into a heavy rainfall event inherits the characteristics already identified for daily precipitation. A "dry spell" is defined as a set of at least 20 consecutive days with accumulated rainfall of less than 10 mm. Figure 5 shows that, as opposed to daily precipitation, the ENSO signal on dry spells is stronger during La Niña events (Q1) than El Niño events (Q4), with a second significant period during the late fall and early winter.

3. Base model

a. Description

Because of the mixed character of daily precipitation, as both a discrete and continuous variable, most available parametric weather generators involve two components (Wilks and Wilby 1999): 1) the occurrence processes (the sequence of dry or wet days) and 2) the intensity processes (the sequence of the nonzero precipitation amounts on wet days). In this study, a wet day is defined as having nonzero (>0 mm) rainfall.

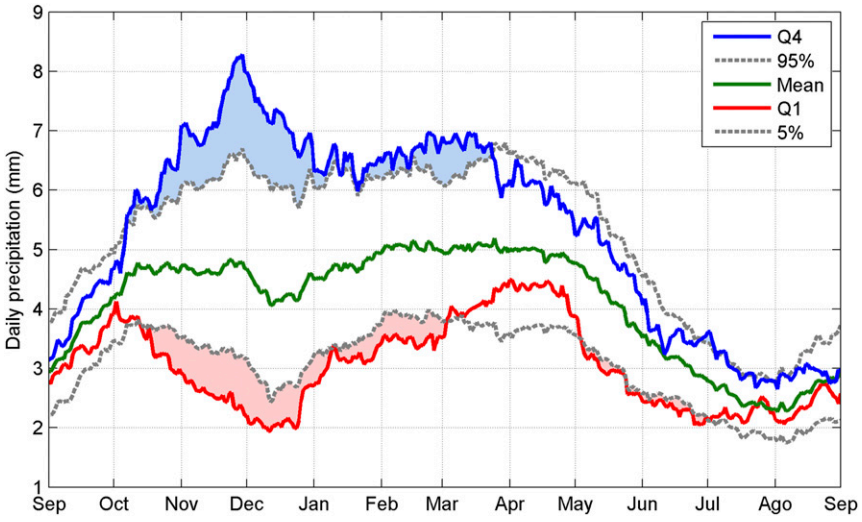

FIG. 3. Annual cycle of daily precipitation obtained from the observed precipitation series for Artigas: climatological mean and ENSO-conditioned extreme quartiles. Dashed lines represent the bottom and top thresholds with 95% significance for the average of ensembles of size equal to the quartiles based on Monte Carlo resampling.

1) PRECIPITATION OCCURRENCE PROCESS

The daily precipitation occurrence model used here is the first-order, two-state Markov chain, according to which the probability of precipitation depends only on whether the previous day was wet or dry. This model is widely used to represent daily precipitation occurrence due to its simplicity (Gabriel and Neumann 1962; Katz 1977a; Richardson 1981; Wilks 1999). It is a two-parameter model that can be defined in terms of the two transition probabilities, $p_{01}(k)$ and $p_{11}(k)$, which are the probability of a wet day following a dry day and the probability of a wet day following a wet day at location k, respectively:

$$p_{01}(k) = P[X_t(k) = 1 | X_{t-1}(k) = 0] \quad \text{and}$$

$$p_{11}(k) = P[X_t(k) = 1 | X_{t-1}(k) = 1]. \tag{1}$$

Here, $X_t(k)$ represents the binary event of precipitation or no precipitation occurring at location k on day t.

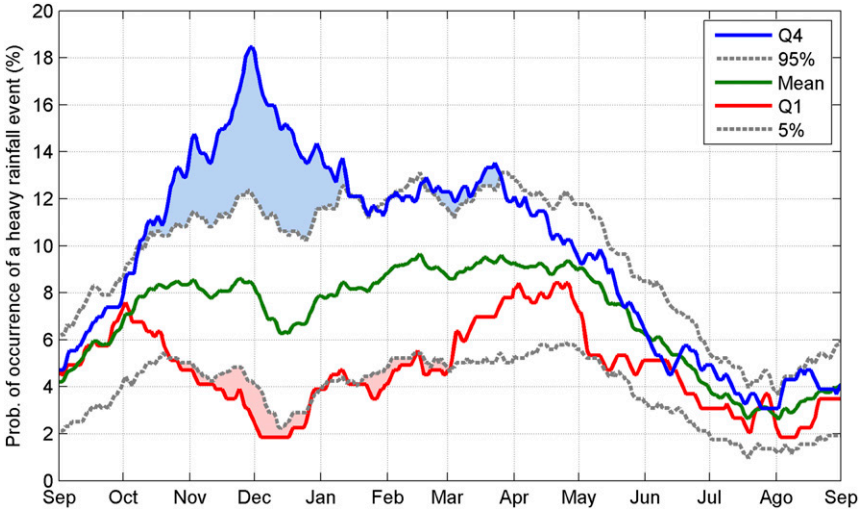

FIG. 4. Annual cycle of the probability of a given day falling into a heavy rainfall event obtained from the observed precipitation series for Artigas: climatological mean and ENSO-conditioned extreme quartiles. Dashed lines represent the bottom and top thresholds with 95% significance for the average of ensembles of size equal to the quartiles based on Monte Carlo resampling.

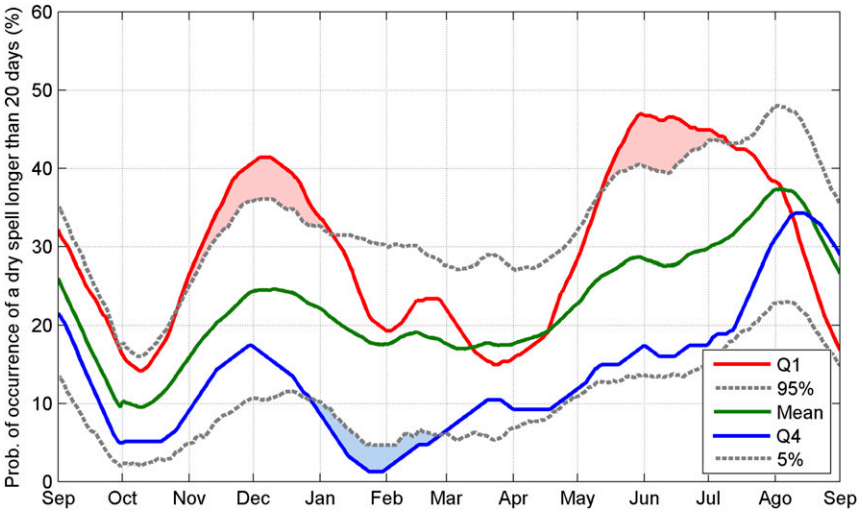

FIG. 5. Annual cycle of the probability of a given day falling into a dry spell longer than 20 days obtained from the observed precipitation series for Artigas: climatological mean and ENSO-conditioned extreme quartiles. Dashed lines represent the bottom and top thresholds with 95% significance for the average of ensembles of size equal to the quartiles based on Monte Carlo resampling.

The two complementary transition probabilities are $p_{00}(k) = 1 - p_{01}(k)$ and $p_{10}(k) = 1 - p_{11}(k)$; then, only two parameters fully determine the model.

This simple model's main limitation is that it generates synthetic rainfall series with very long dry spells (runs of consecutive dry days) too infrequently (Buishand 1977; Racsko et al. 1991; Wilks 1999). It has been found that this deficiency can be addressed by considering Markov chains of higher order (Chin 1977; Coe and Stern 1982; Wilks 1999), but these models are more complex and require more parameters for validation (a kth-order, two-state Markov process is defined by 2^k parameters); therefore, they are not discussed here.

2) PRECIPITATION INTENSITY PROCESS

Given the occurrence of a wet day, daily nonzero precipitation amount can be modeled using many statistical distributions (exponential, gamma, mixed exponential, lognormal, and Weibull distributions). The most dominant statistical feature of daily precipitation amounts is that their distribution is strongly positive skewed (Wilks and Wilby 1999). This work considers the two-parameter gamma distribution with a probability density function:

$$f(x) = \frac{(x/\beta)^{\alpha-1} e^{-x/\beta}}{\beta\Gamma(\alpha)}; \quad x, \alpha, \beta > 0\,. \tag{2}$$

The variable x is the daily precipitation amount (mm), α and β are the two distribution parameters (shape and scale parameters, respectively), and $\Gamma(\alpha)$ indicates the gamma function evaluated at α.

The gamma distribution is one of the most popular choices for representing distributions of daily nonzero precipitation amounts in stochastic weather models (Katz 1977b; Stern and Coe 1984; Wilks 1992; Aksoy 2000; Baigorria and Jones 2010).

Common assumptions are that daily nonzero precipitation amounts are identically distributed and independent of both the occurrence process and of rainfall amounts on previous and/or successive days.

We also evaluated (not presented) a three-parameter mixed exponential distribution (mixing probability α and scale parameters β_1 and β_2). Even though this model delivers marginally better performance than the gamma distribution, it was deemed that the improvement does not justify the use of a less parsimonious model. This may be due to the relatively narrow spectrum of climatic regimes in Uruguay, in particular with no dry season anywhere.

3) SEASONAL VARIATION OF MODEL PARAMETERS

To capture the seasonal variation in precipitation, we determine the mean annual cycle of the model parameters. A separate set of parameters is estimated for each calendar day using a centered moving window of ±30 days, and sampling data from all days, as well as from every year, falling within such a window (Rajagopalan et al. 1996).

For each calendar day, parameter estimates for both the intensity and occurrence models are obtained using the maximum likelihood method.

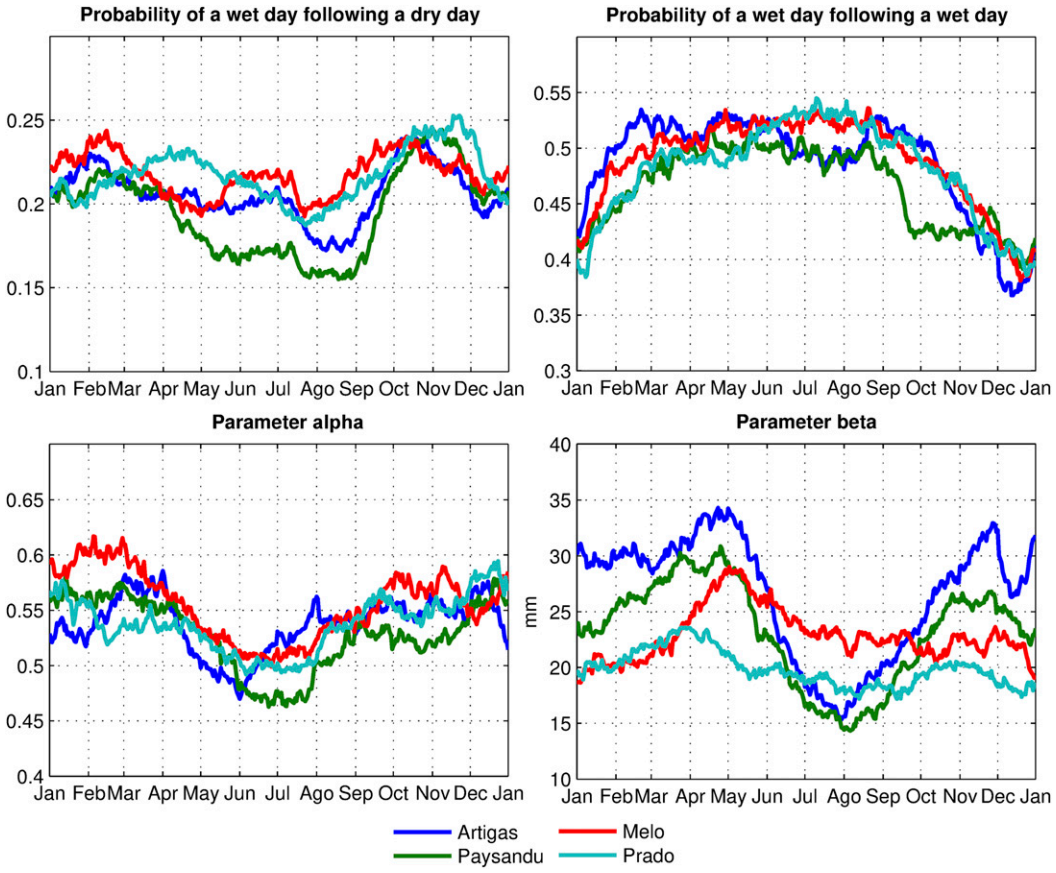

FIG. 6. Annual cycle of model parameters (p_{11}, p_{01}, α, and β) obtained for the Artigas (northern), Paysandú (western), Melo (eastern), and Prado (southern) stations.

As an example, Fig. 6 shows the mean annual cycle of model parameters (p_{01}, p_{11}, α, and β) obtained for the Artigas (northern), Paysandú (western), Melo (eastern), and Prado (southern) stations for the 1981–2009 period.

This approach smoothly captures the seasonal cycle of model parameters with the fewest assumptions; no fixed seasons or functions, harmonic or otherwise, are imposed. No attempt is made to independently calibrate a large number of parameters either; the methodology is data driven, with the vast majority of the data reused in the determination of parameters from one day to the next. It does implicitly assume the interannual stationarity of the model parameters. This assumption will be relaxed in section 4, in order to allow for interannual variability of model parameters associated with a climate index.

b. *Evaluation*

To evaluate the performance of the base model, we simulated 100 realizations of a 29-yr (same length as the common historical record) synthetic series of daily precipitation for each weather station.

The stochastic precipitation model considered here (Markov+Gamma) has been shown to yield practically exact reproductions of the average number of wet days and the average wet-day amount (Wilks 1999; Wilks and Wilby 1999). Additionally, our base model with seasonally varying parameters also captures, by construction, the climatological seasonal cycle of precipitation.

The model should also closely reproduce the mean of aggregated quantities such as monthly (or seasonal) total precipitation (Katz and Parlange 1996; Grondona et al. 2000). However, it is well known that standard weather generators fitted to time series of daily precipitation tend to underestimate the interannual variance of aggregated quantities such as monthly, seasonal, or annual total precipitation (Katz and Parlange 1998; Wilks 1999). This phenomenon, in which the observed variance exceeds the one obtained from the fitted model, is termed ‘‘overdispersion.’’

In this sense, Fig. 7 shows the spatial variability of the overdispersion coefficient (Wilks 1999), expressed on a percentage basis, for the September–August accumulated precipitation:

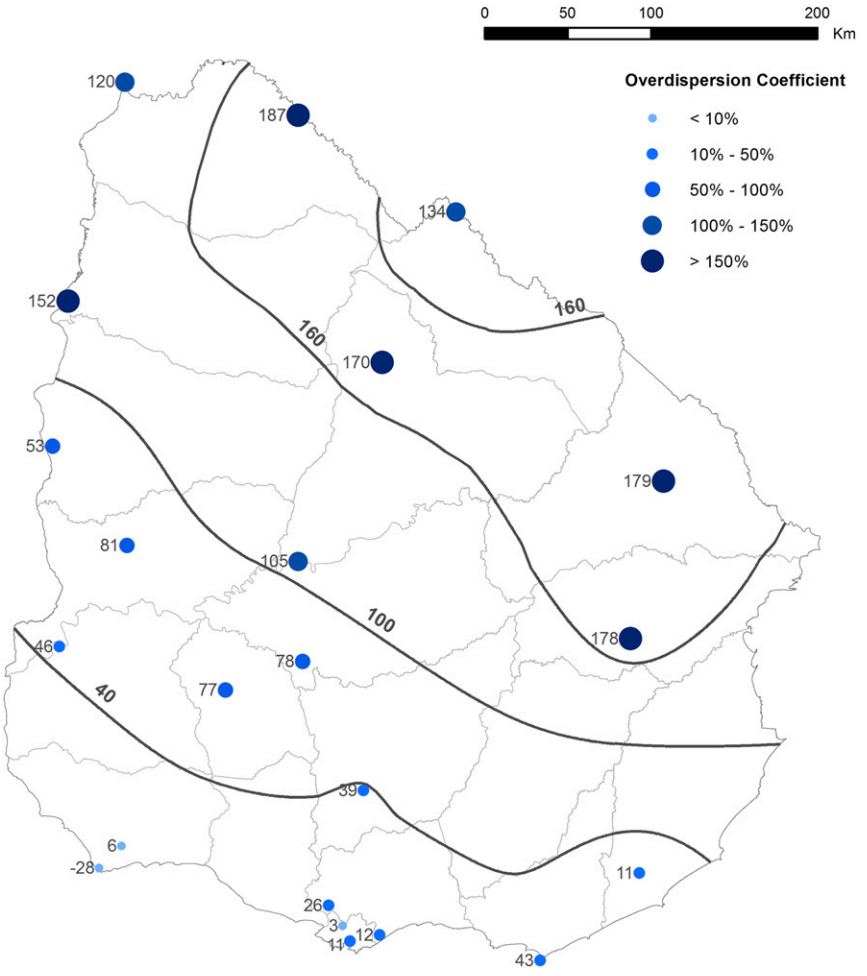

FIG. 7. Overdispersion coefficient associated with simulations with the base model (Sim 1) for September–August accumulated precipitation.

$$\text{Overdispersion Coef} = \left(\frac{\text{Observed Variance}}{\text{Modeled Variance}} - 1\right) \times 100\%. \quad (3)$$

Overdispersion presents a southwest–northeast gradient, with the largest positive values being over 170%. This confirms that the model does not adequately capture the amplitude of the variability at interannual time scales, which was expected since such variability is not explicitly considered. Moreover, it is evident that the spatial pattern in Fig. 7 is quite similar to that in the right panel of Fig. 2, confirming that ENSO-related interannual variability is dominant.

4. Proposed model

We next present a modification of the Markov+Gamma base model in which the parameters (p_{01}, p_{11}, α, and β) can vary associated with a climate index. The approach is to generate daily synthetic time series of deviations of the model parameters around their climatological seasonal cycle associated with the evolution of a climate index that, in the scenario of a real-life application, has to be independently predicted.

We use the daily N3.4-NDJ time series presented in section 2b as the climate index. Nevertheless, the methodology is completely general and could be readily transferable to other climate indices, representatives of other climate modes, or as part of a downscaling technique (Nicholas and Battisti 2012; Guo et al. 2014).

The proposed methodology comprises the following steps:

1) Construct daily time series of the model parameters associated with the climate index using the ''analog days'' technique.
2) Based on the daily time series of model parameters and the climate index, fit a vector autoregressive

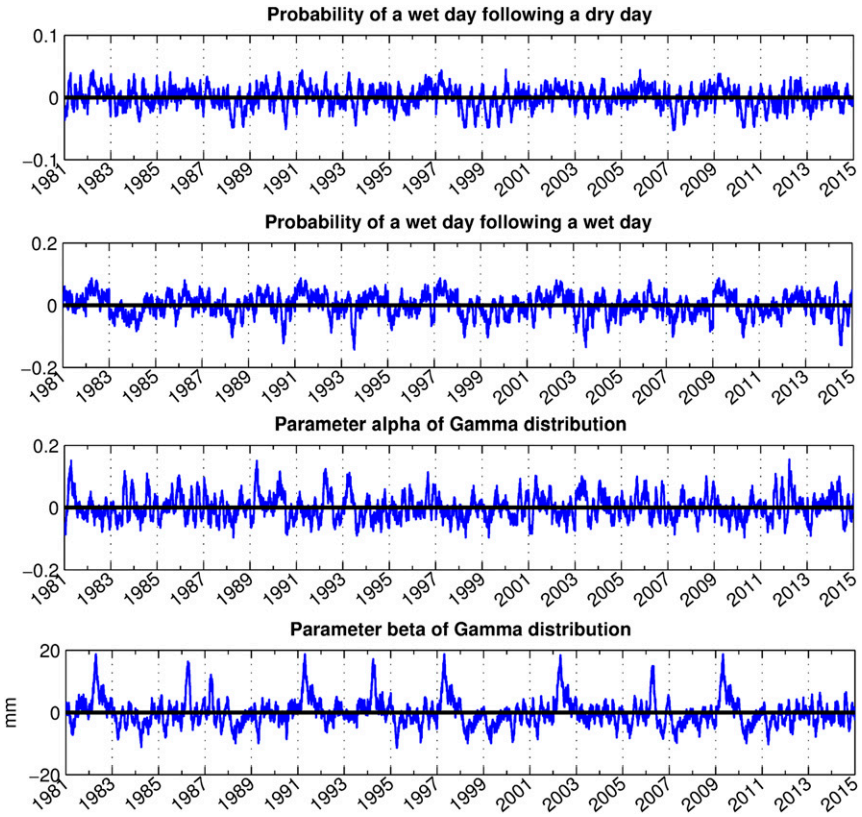

FIG. 8. Parameter anomalies time series (September 1981–August 2015) constructed based on the N3.4-NDJ index using the analog days technique.

(VAR) linear model in Gaussian space (Chaer 2005) for model parameters taking seasonal variability into account.

3) Generate synthetic time series of model parameters.
4) In turn, generate synthetic time series of daily precipitation.

Results are shown for the Artigas weather station, among those with the strongest ENSO signal (Fig. 2) and highest overdispersion (Fig. 7).

a. *Time series of the model parameters associated with the climate index*

For any given day in the time series, we first need to define a set of "analog days" that is large enough to be able to estimate the weather generator parameters (p_{01}, p_{11}, α, and β) and is composed of days that are "similar" enough to the day in question. By similar enough, we mean close enough in time of year and in the value of the climate index.

The underlying assumption is that, in view of the known relation between ENSO and precipitation in Uruguay (Pisciottano et al. 1994), the historical data distribution limited to the analog days better represents the expected value as compared to the entire historical set.

The determination of the size of the window that defines the analog days, both in the calendar year and in the climate index, represents a compromise between the sample size and similarity of analog days.

We used a centered moving time window of ±30 calendar days as before [see section 3a(3)]. Regarding the climate index, the window contains 25% of the days with more similar values, it is centered around the value of the given day when possible, and it coincides with the extreme quartiles when the value falls into the top octiles. Therefore, the subset of analog days has a total length of 25% × (30 + 1 + 30) days × 35 years ≈ 533 days, within which approximately 28% (150 days) correspond to wet days (>0 mm).

Once the time series of model parameters (p_{01}, p_{11}, α, and β) associated with the climate index are computed, we calculate their deviations ("parameter anomalies") from their climatological seasonal cycle (shown in Fig. 6).

The time series thus obtained (Fig. 8) attempt to capture the variability of the model parameters associated with the climatic index used, in this case the

TABLE 1. Statistics of ENSO-conditioned model parameters series: Mean and std dev of annual cycle and std dev of parameter anomalies (constructed and synthetic).

		Std dev		
Parameter	Mean	Mean annual cycle	Constructed series	Synthetic series
p_{01}	0.21	0.016 (7.6%)	0.016 (7.9%)	0.018 (8.6%)
p_{11}	0.48	0.037 (7.6%)	0.035 (7.2%)	0.035 (7.2%)
α	0.55	0.027 (4.9%)	0.038 (7.0%)	0.041 (7.5%)
β (mm)	26.3	5.3 (20.2%)	4.3 (16.5%)	5.1 (19.6%)

N3.4-NDJ, through sampling of analog days in the observed rainfall record.

To quantify the potential impact of the added variability, Table 1 shows the mean value of each model parameter, the standard deviation (std dev) of its mean annual cycle, and the standard deviation of the series of parameter anomalies previously obtained. Both deviations are of the same order of magnitude, confirming that the amplitude of the interannual variability associated with ENSO is as important as the seasonal cycle itself. The last column in Table 1 will be discussed in section 5.

b. *Autoregressive linear model in Gaussian space for model parameters*

We then proceed to fit a VAR linear model in Gaussian space, estimated considering seasonal variability. The methodology is similar to that employed in Maciel et al. (2015), and the following text is derived from there with the required adaptations and minor modifications.

The model first constructs nonlinear functions, and their inverse, to transform daily histograms of parameter and climate index anomalies (real space) into normal distributions (Gaussian space) through quantile matching. In no way do we imply that the original distributions are normal; the convenience of working in Gaussian space simplifies the modeling that is introduced next.

A first-order vector autoregressive model VAR(1) is calibrated in Gaussian space, incorporating the N3.4 index:

$$\begin{bmatrix} p_{01} \\ p_{11} \\ \alpha \\ \beta \\ \text{N3.4} \end{bmatrix}_{k+1} = [\mathbf{A}_k(5\times5)] \times \begin{bmatrix} p_{01} \\ p_{11} \\ \alpha \\ \beta \\ \text{N3.4} \end{bmatrix}_{k} + [\mathbf{B}_k(5\times5)] \times \mathbf{w}_k(5\times1). \quad (4)$$

Parameters of the $(k+1)$th day are computed multiplying parameters of the kth day by matrix $\mathbf{A}_k$, which captures the auto- and cross correlations with a lag of 1 day, plus correlated Gaussian white noise, $\mathbf{B}_k \times \mathbf{w}_k$. The coefficients of matrix $\mathbf{A}_k$, which varies with the day of the year (1–365), are calibrated using the daily time series of the model parameter anomalies and the N3.4 index (1981–2015) in Gaussian space. This enables the system to capture the (strong) seasonality of the relation between N3.4 and the parameters. Once $\mathbf{A}_k$ is known, the coefficients of matrix $\mathbf{B}_k$, which also vary with the day of the year, are determined so that the covariance of the synthetic time series coincides with the observed covariance (Chaer 2013). When available time series are short, the computation of $\mathbf{A}_k$ and $\mathbf{B}_k$ for every calendar day again requires the consideration of a window centered around the given day to give robust estimations.

As the linear transformation of Gaussian processes is also Gaussian, the shape of the parameters' daily histograms is conserved once the inverse functions are applied and the synthetic time series in "real space" are obtained. In addition, 1-day correlations and autocorrelations in Gaussian space are maintained.

Figure 9 presents the distribution of the model parameter anomalies (conditioned by ENSO) prior to normalization. Note that, in this case, they are quite close to normal, which implies that the correlations are approximately conserved also in real space.

As an example, Table 2 shows the coefficients of matrices $\mathbf{A}$ and $\mathbf{B}$ without considering seasonal variability (only one matrix for the entire year).

Additionally, Fig. 10 shows the seasonal variation of one of the key coefficients [β, N3.4] of matrix $\mathbf{A}_k$ as a function of the length of the sampling window (5, 7, and 10 days); the value without seasonal variability (0.027) is also included. This coefficient represents the influence of ENSO on the β parameter, which dominates the amplitude of precipitation amounts. Figure 10 highlights the importance of considering the seasonality in matrix $\mathbf{A}_k$. It also shows that the impact of the sampling window, which was set at 7 days, is relatively minor.

c. *Synthetic time series of model parameters*

Equation (4) could either be used in a "free" mode, synthesizing all five variables, or prescribing the trajectory

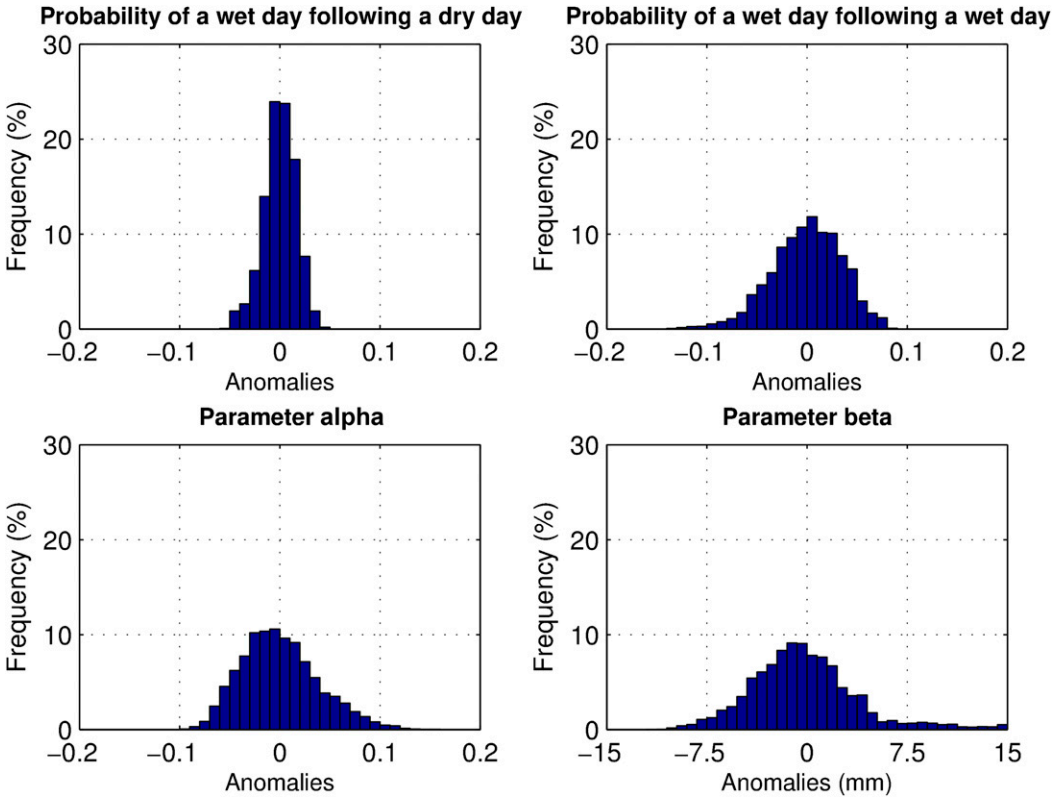

FIG. 9. Distribution of the model parameter anomalies prior to normalization.

of the climate index as in Maciel et al. (2015). The latter is the intended use of the model, which in no way attempts to capture the dynamics of the climate index, but rather generates many possible realizations of p_{01}, p_{11}, α, and β, conditioned to a certain evolution of ENSO. That is why the cells in italics in Table 2 (last row) are not used in the simulation of the parameter series.

TABLE 2. Coefficients of matrices **A** and **B** of the VAR(1) model without considering seasonal variability. The italic numerical values are not used in the simulation of the parameter series.

	p_{01}	p_{11}	α	β	N3.4
			Matrix **A**		
p_{01}	0.938	0.003	0.024	0.024	0.007
p_{11}	0.015	0.932	0.000 03	0.025	0.011
α	−0.006	0.011	0.961	−0.001	−0.002
β	0.017	0.003	−0.009	0.931	0.027
N3.4	*0.006*	*−0.003*	*−0.001*	*−0.003*	*0.998*
			Matrix **B**		
p_{01}	0.323	−0.014	0.007	−0.014	−0.014
p_{11}	−0.014	0.307	−0.007	0.019	0.017
α	0.007	−0.007	0.286	−0.075	−0.003
β	−0.014	0.019	−0.075	0.296	0.009
N3.4	*−0.014*	*0.017*	*−0.003*	*0.009*	*0.087*

One hundred realizations of 34-yr-long synthetic time series of model parameter anomalies were generated using the observed evolution of N3.4-NDJ.

The correlations between N3.4-NDJ and the synthetic series of model parameters were compared to the corresponding correlations of the time series constructed using the "analog days" technique (used to calibrate the model itself). In the case of the synthetic series, we considered the average of the correlations calculated for each of the 100 realizations. Table 3 shows that the synthetic series manage to reproduce the structure of the correlations of the constructed series, when the latter are significant, but with a bias to lower (absolute) values.

d. Synthetic time series of daily precipitation

Finally, we generate the synthetic time series of daily precipitation based on the simulated time series of model parameters, using the Markov+Gamma model presented in section 3. The results are shown and analyzed in the next section.

The methodology presented thus far makes use of all the available historical record. Consequently, the resulting model cannot be validated against observations during the same period. Since all climate predictions, which is what we want to encapsulate in the proposed model, are

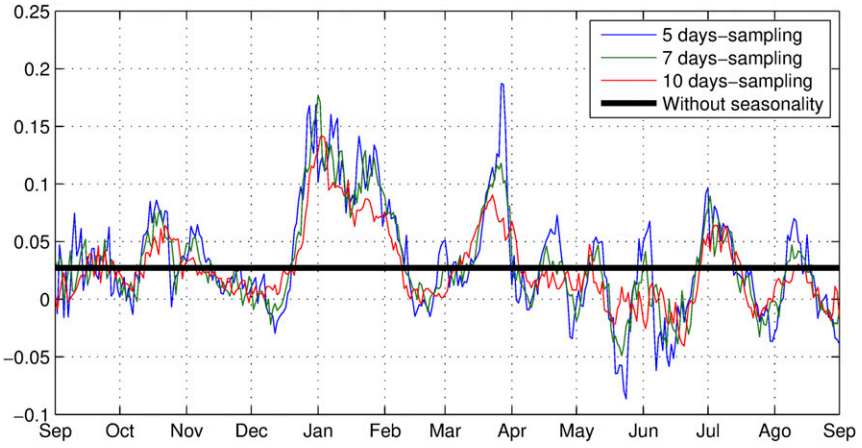

FIG. 10. Seasonal variation of the coefficient [β, N3.4] of matrix $\mathbf{A}_k$ in the VAR(1) model as a function of the length of the overlap window.

probabilistic in nature, the performance cannot be judged on the basis of a low number of seasons. In addition, the period for which data are available is relatively short, rendering the strategy of separating calibration and validation periods unfeasible. We, therefore, turned to a leave-one-out approach for validation, taking advantage that the ''analog days'' technique does not require continuity in the data.

Accordingly, the entire methodology (construction of the parameter time series, calibration of the VAR model, simulation of the WG parameters, and, in turn, precipitation) was repeated 34 times, once per September–August year, following a strict leave-one-out approach, whereas the observed precipitation data for each given year are not used at all. Every result presented in the next section, and compared to observations, is done in leave-one-out validation mode.

5. Results

To evaluate the performance of the proposed methodology we conducted three sets of simulations:

1) Sim1: One hundred 34-yr-long simulations of daily precipitation with the base model as originally presented in section 3, without incorporating interannual variability in the model parameters;
2) Sim2: One hundred 34-yr-long simulations of daily precipitation based on the parameters' time series constructed using the analog-days technique (conditioned by the N3.4 index) and used to calibrate the improved model, thus, representing the model in calibration mode; it is included only as a reference;
3) Sim3: One hundred 34-yr-long simulations of daily precipitation based on the improved model with varying parameters in association with the observed evolution of the N3.4-NDJ index in the 1981–2015 period. One daily precipitation series was simulated from each realization of the synthetic time series of model parameters.

TABLE 3. Correlation of N3.4-NDJ index with the model parameter anomalies for the constructed and synthetic time series.

Parameter	Constructed series	Synthetic series
p_{01}	0.36	0.21
p_{11}	0.50	0.43
α	−0.08	0.13
β	0.59	0.57

a. *Parameters: Stratification plots*

The last column in Table 1 shows the standard deviation of the synthetic series of model parameter anomalies, confirming that the methodology fully captures the amplitude of interannual variability of the parameters associated with ENSO.

Next, we analyzed the seasonal variation of the ENSO signal in the model parameters. In addition to their applied interest, the parameters may also be related to the nature and frequency of precipitating systems in a given region.

We determine the mean annual cycle of the model parameters (p_{01}, p_{11}, α, and β) for each quartile according to the N3.4-NDJ index (similar to Figs. 3–5). Figure 11 shows the results obtained for the constructed parameter time series (8 years per quartile) used in Sim2 (left column) and the synthetic series of model parameters (8 × 100 years per quartile) used in Sim3 (right column). It also includes, in dashed lines, the extreme quartiles derived from the simulated daily precipitation, with Sim2 and Sim3,

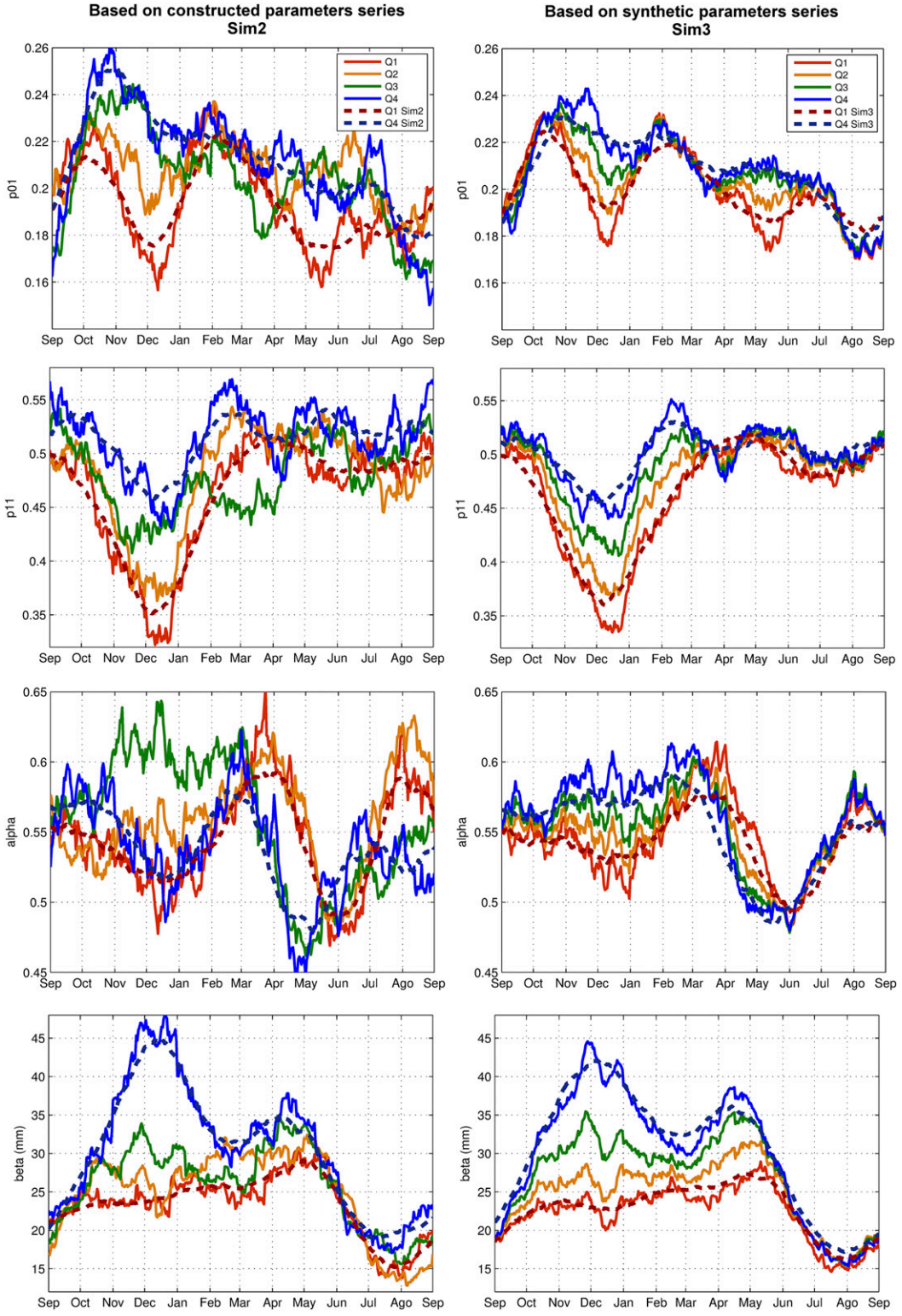

FIG. 11. Mean annual cycle of the model parameters for each quartile according to the N3.4-NDJ index for the (left) constructed (Sim2) and (right) synthetic (Sim3) parameters time series (see text).

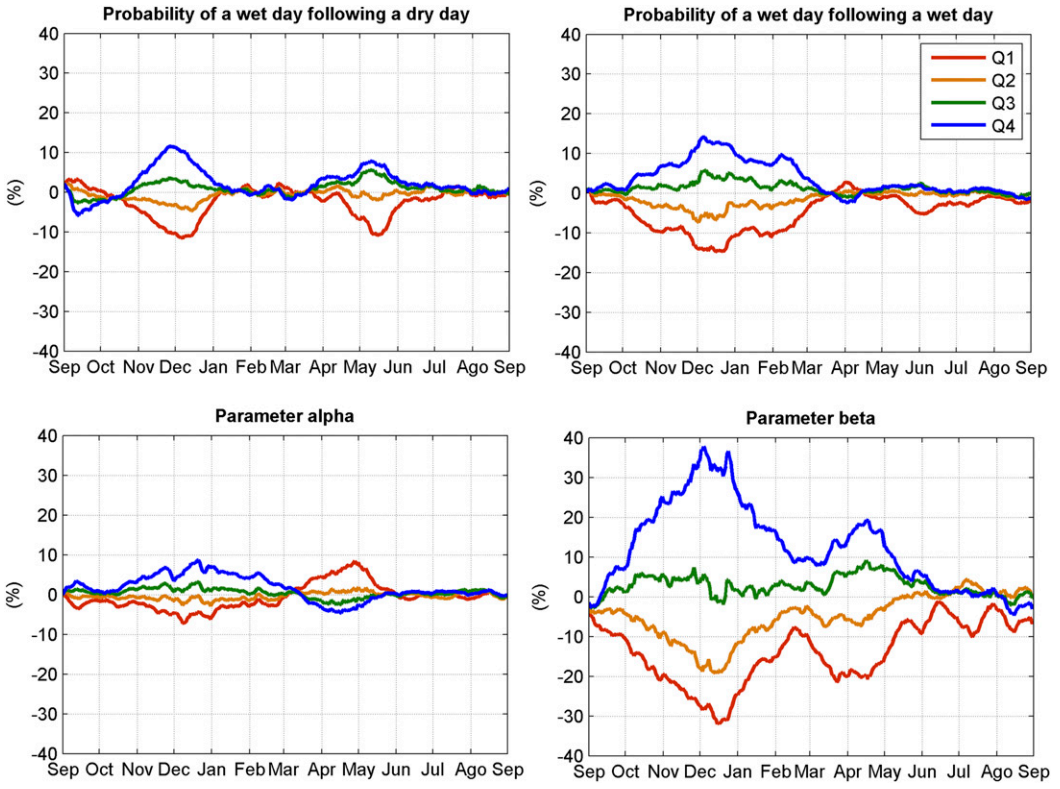

FIG. 12. Mean annual cycle of the normalized model parameter anomalies for each quartile according to the N3.4-NDJ index, obtained from the synthetic series of model parameters.

respectively, considering a centered moving window of ±30 days (8 × 100 years per quartile).

In general, we observe that Q1 most stratifies the conditional probabilities of precipitation, whereas Q4 differs substantially from the other quartiles in the parameter β (which dominates the amplitude of precipitation amounts). These stratifications are in the expected direction: Q1 (La Niña events) has negative associated rainfall biases in Uruguay and Q4 (El Niño events) has positive ones (see Fig. 3). For the parameter α there is no clear distinction between the different quartiles. Also, it is the parameter for which the left and right columns most differ. It should be noted that this analysis does not have an associated test to identify statistically significant differences among the quartiles. Such tests are implemented for the observed and simulated precipitation series (see sections 2b and 5c).

One distinctive difference of the cycles obtained based on the synthetic series of model parameters (Fig. 11, right column) is that they are monotonically stratified in quartiles, with notable seasonal variations (a feature best captured in Fig. 12), which is not strictly the case in the left column, especially when ENSO stratification is weak as is the case for parameter α. Cycles obtained from simulated precipitation series (dashed lines) are much smoother but follow the respective driving parameters.

Figure 12 shows the mean annual cycle of the model parameter anomalies for each quartile according to the N3.4-NDJ index, obtained from the synthetic series of model parameters (8 × 100 years per quartile). It is the same information conveyed in the right column of Fig. 11, but presented as normalized deviations of the model parameters from their climatological seasonal cycle (presented in Fig. 6), for better visualization of the relative amplitude of the (seasonally varying) ENSO signal on each parameter.

The seasonality of ENSO's impact on precipitation in Uruguay has been established previously (Cazes-Boezio et al. 2003): it is strongest during austral spring (October–December), recedes in peak summer (January–February), and returns weakly in fall–winter (March–July). Parameters p_{01}, p_{11}, and β present clear stratifications that roughly follow this pattern with subtle differences. Parameter β shows the stratification with larger relative amplitude. It has its strongest signal during the local spring and extends until winter (July–August), with lower deviations during February. Parameters p_{01} and p_{11} also present a stronger and longer stratification during austral spring, as compared to fall. Parameter p_{01} shows a pronounced break in the

TABLE 4. Mean, variance, and fraction of variance linearly associated with ENSO for the Sep–Aug and NDJ accumulated precipitation at the Artigas station. The variance and associated overdispersion in simulated series with Sim1 and Sim3 are shown.

Period	Mean obs (mm)	Variance obs (mm^2)	N3.4-NDJ R^2	Variance Sim1 (mm^2)	Variance Sim3 (mm^2)
NDJ	399	39 645	0.48	20 331 (95.0%)	44 353 (−10.6%)
Sep–Aug	1503	198 256	0.35	69 105 (186.9%)	139 696 (41.9%)

signal in late summer and early fall. Finally, parameter α shows a weak signal in the spring (October–December) and peak summer, which reverses sign during the fall.

Regardless of the intensity and seasonality of the ENSO signal, the quartiles Q1, Q2, Q3, and Q4 are always orderly stratified for all parameters, except when the signal is very weak. This property is not strictly verified in the constructed series.

b. Precipitation variance

We then proceed to evaluate the performance of the proposed model. In particular, we focus on the aspects in which the base model, without incorporating interannual variability in the parameters, performs worst (section 3b): the seasonal and interannual precipitation variability.

Table 4 shows the observed and simulated interannual variance of Artigas rainfall accumulated over ENSO years (September–August) and NDJ, the season with the strongest ENSO signal. Table 4 also presents the square of the correlation coefficients in Fig. 2 for Artigas, which can be interpreted as the fraction of the variance of precipitation explained by a linear relation to ENSO. Multiplying columns 3 and 4 in Table 4 thus gives an estimate of the amplitude of ENSO variance in the record: 19 030 and 69 390 mm^2 for the NDJ and September–August periods, respectively.

Sim1, which does not explicitly model interannual variability, has approximately one-half (one-third) of the observed variance for the trimester (year), which confirms that the overdispersion problem grows with the averaging period in these models. We see that the proposed model (Sim3) doubles the variance of Sim1 at the annual time scale and more than doubles it in the season of strongest ENSO influence (NDJ). Since the WG variability that Sim3 inherits from Sim1 is entirely independent from the newly incorporated result associated with ENSO, the respective variances can be considered additive. Therefore, the magnitude of the ENSO-related variance added can be obtained by subtracting that of Sim1 from that of Sim3, giving 24 022 and 70 591 mm^2 for the NDJ and September–August periods, respectively.

In summary, Sim3 captures almost the exact amount of the ENSO-linearly related variance in the record for September–August years and overestimates it during the season of peak signal (NDJ).

c. Shifts in precipitation associated with ENSO

For the proposed model to be useful in probabilistic, prediction mode, we need to show that it smoothly captures the time-evolving shift in key precipitation statistics associated with the influence of the climate index, the prediction of which has to be independently provided.

For such purpose, we analyzed the stratification associated with ENSO for the three rainfall-based statistics presented in section 2b based on the simulations in leave-one-out validation mode.

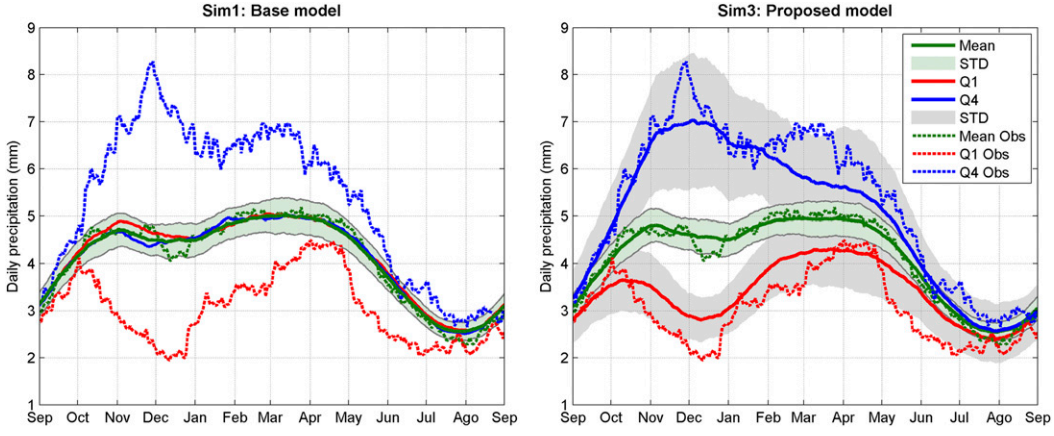

FIG. 13. Annual cycle of observed (dotted) and simulated (solid) daily precipitation for Artigas with (left) Sim1 and (right) Sim3: 34-yr climatology and 8-yr ensemble conditioned to ENSO extreme quartiles. In the case of simulations, ±1 std dev among 100 realizations is shaded both for the climatology and the quartiles of Sim3.

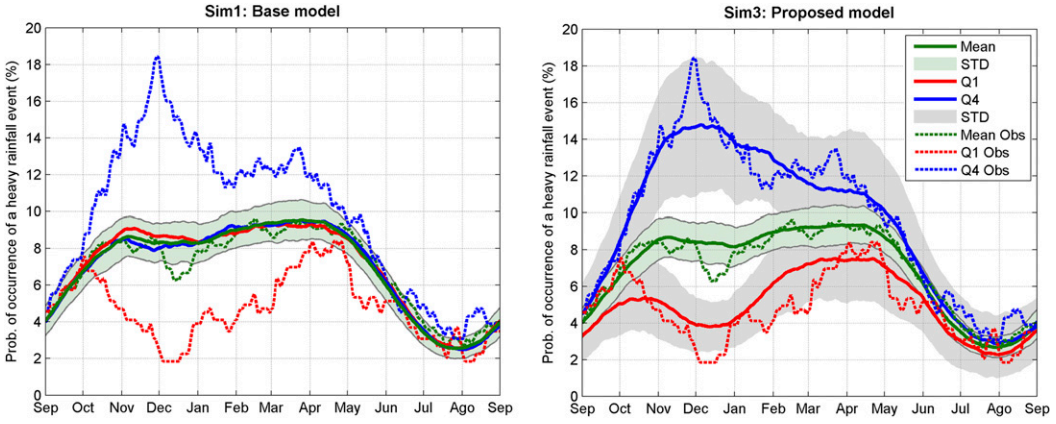

FIG. 14. Annual cycle of observed (dotted) and simulated (solid) probability of a given day falling within a heavy rainfall event for Artigas with (left) Sim1 and (right) Sim3: 34-yr climatology and 8-yr ensemble conditioned to ENSO extreme quartiles. In the case of simulations, ±1 std dev among 100 realizations is shaded both for the climatology and the quartiles of Sim3.

Figure 13 shows the annual cycle of daily precipitation for Artigas derived from Sim1 (left panel) and Sim3 (right panel) for all years (mean) and for ensembles conditioned by the extreme quartiles of the N3.4-NDJ index (Q1 and Q4), considering a centered moving window of ±30 days. We do have 100 annual cycles, one per 34-yr-long simulation, so we present the mean plus and minus one standard deviation among the simulations (shaded). The figure also includes, in dashed lines, the cycles derived from the single 34-yr observed record (as in Fig. 3). In the left panel we show the results with the base model (with seasonality but no interannual variability), which captures the seasonal cycle quite well, not only for daily precipitation but also for higher-order statistics (heavy rainfall events and dry spells; Figs. 14 and 15, respectively). However, statistics conditional to ENSO years are naturally entirely missed, since the base model has no explicit interannual signal and the randomness intrinsic to the WG is far too small at the interannual time scale. The results with the proposed model are consistent with the behavior previously observed in the cycles of the model parameters (Figs. 11 and 12). The synthetic series reproduced the signal identified in the observed ones, but with a slightly smaller amplitude.

Figure 14 shows that the seasonality of the ENSO signal in the probability of a given day falling into a heavy rainfall event is, again, well captured by the proposed model, but its amplitude is somewhat reduced. The mean annual cycle of the probability of a given day falling into a 20-day-long spell is quite well reproduced;

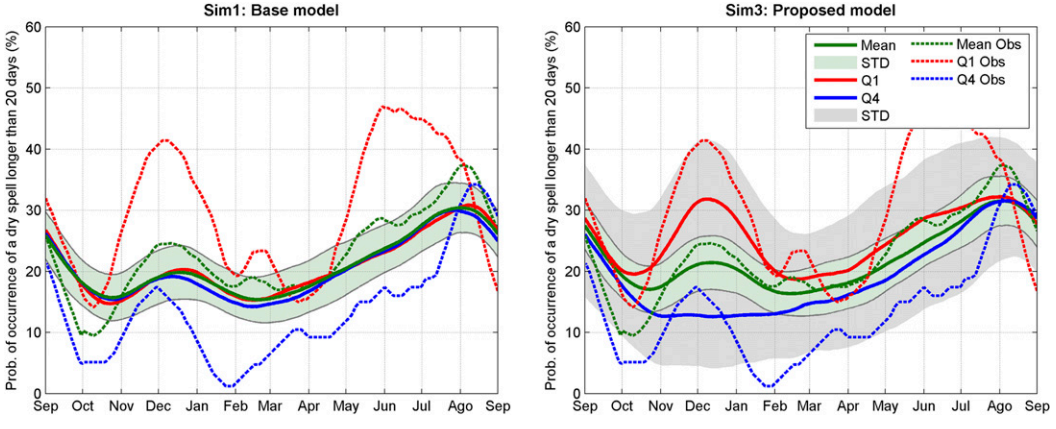

FIG. 15. Annual cycle of observed (dotted) and simulated (solid) probability of a given day falling within a dry spell longer than 20 days for Artigas with (left) Sim1 and (right) Sim3: 34-yr climatology and 8-yr ensemble conditioned to ENSO extreme quartiles. In the case of simulations, ±1 std dev among 100 realizations is shaded both for the climatology and the quartiles of Sim3.

however, such events are not easily captured by first-order models. The conditioning of ENSO is also evident in the synthetic series, but the seasonality and amplitude deviate from the observed record (Fig. 15). The longer the spell and the less frequent the event, the worse the performance of the model (not shown). It has to be kept in mind that the weather generator is not specifically designed to capture extremes and should not be used for such purposes.

6. Summary and conclusions

We have proposed a stochastic daily precipitation generator that smoothly incorporates a climate index to reflect associated and gradually varying shifts in simulated precipitation statistics. The weather generator is based on a first-order, two-state Markov chain for simulating the occurrence of daily precipitation and a gamma distribution for computing the nonzero daily precipitation amounts. Therefore, it has four parameters that are, in turn, allowed to vary daily following a vector autoregressive linear model in Gaussian space that simulates the parameters' deviations from their climatological seasonal cycles. This model is forced by the independently predicted evolution of a climate index and captures how the model parameters and, in turn, the precipitation are shifted by the associated climate signal.

The proposed methodology comprises four steps:

1) Construct daily time series of the Markov+Gamma model parameters associated with the climate index using the ''analog days'' technique.
2) Based on the daily time series of model parameters and the climate index, fit a first-order VAR linear model in Gaussian space estimated considering the seasonal variability.
3) Generate synthetic time series of model parameters using the VAR(1) model previously fitted.
4) Generate synthetic time series of daily precipitation using the Markov+Gamma model.

In this case, we use the N3.4 index to account for the influence of the ENSO phenomena on precipitation in Uruguay. However, the methodology is completely general and could be readily transferable to other regions provided there is significant seasonal predictability associated with a scalar index that could either represent a climate mode or result from a climate prediction downscaling algorithm.

The results show that the proposed methodology successfully captures ENSO's impact on the model parameters and, consequently, on daily precipitation and key statistics as it gradually emerges and recedes. The resulting stratifications are in the expected directions, where Q1 has negative associated rainfall biases in Uruguay and Q4 has positive ones. The results roughly follow the seasonal pattern previously established by Cazes-Boezio et al. (2003): the ENSO signal is strongest during austral spring, recedes in peak summer, and returns weakly in fall–winter. Parameter β shows the stratification with larger relative amplitude, followed by the conditional probabilities p_{01} and p_{11}. One distinctive feature of the cycles obtained based on the synthetic series of model parameters is that, regardless of the intensity and seasonality of the signal, they are monotonically stratified in quartiles, which is not strictly verified in the constructed series.

By successfully capturing most of ENSO-related variability, the proposed model greatly reduces the ''overdispersion'' problem, a well-known limitation of standard weather generators (from 187% in the base model to 42% for the accumulated September–August rainfall). Of course, the part of the variability that is not associated with the particular climate index used (in this case N3.4) is beyond the scope of this method.

These results open interesting opportunities for the application of seasonal climate forecasts in several process-based models (e.g., crop, hydrological, electric power system, water resources), which may be used to inform the decision-making and planning processes for managing climate-related risks.

Acknowledgments. We very much appreciate the reviewers' comments and suggestions whose input strongly improved the manuscript. The first author enjoyed a master's scholarship awarded by the National Agency for Research and Innovation (ANII) that greatly contributed to this work (POS_NAC_2012_1_8793). Part of the work was conducted within the framework of the Ministry of Livestock, Agriculture and Fisheries's (MGAP) Development and Adaptation to Climate Change (DACC) Project, financed by the World Bank. We are grateful to InUMet and INIA for the availability of the daily precipitation data.

REFERENCES

Aceituno, P., 1992: El Niño, the Southern Oscillation, and ENSO: Confusing names for a complex ocean–atmosphere interaction. *Bull. Amer. Meteor. Soc.*, **73**, 483–485, https://doi.org/10.1175/1520-0477-73.4.483.

Ailliot, P., D. Allard, and V. Monbet, 2015: Stochastic weather generators: An overview of weather type models. *J. Soc. Fr. Stat.*, **156**, 101–113.

Aksoy, H., 2000: Use of gamma distribution in hydrological analysis. *Turk. J. Eng. Env. Sci.*, **24**, 419–428.

Baigorria, G. A., and W. J. Jones, 2010: GiST: A stochastic model for generating spatially and temporally correlated daily rainfall data. *J. Climate*, **23**, 5990–6008, https://doi.org/10.1175/2010JCLI3537.1.

Brissette, F. P., M. Khalili, and R. Leconte, 2007: Efficient stochastic generation of multi-site synthetic precipitation data. *J. Hydrol.*, **345**, 121–133, https://doi.org/10.1016/j.jhydrol.2007.06.035.

Buishand, T. A., 1977: Stochastic modelling of daily rainfall sequences. Mededelingen Landbouwhogeschool Rep. 77-3, Wageningen, Netherlands, 211 pp., http://edepot.wur.nl/288686.

Cazes-Boezio, G., A. W. Robertson, and C. R. Mechoso, 2003: Seasonal dependence of ENSO teleconnections over South America and relationships with precipitation in Uruguay. *J. Climate*, **16**, 1159–1176, https://doi.org/10.1175/1520-0442(2003)16<1159:SDOETO>2.0.CO;2.

Chaer, R., 2005: Modelo de series correlacionadas CEGH. Curso SimSEE, Instituto de Ingeniería Eléctrica, Facultad de Ingeniería, Universidad de la República, Montevideo, Uruguay, 9 pp., https://simsee.org/simsee/curso2010/Cap9_sintetizadorCEGH.pdf.

——, 2013: Fundamentos del modelo CEGH de procesos estocásticos multivariables. Instituto de Ingeniería Eléctrica Tech. Rep., Facultad de Ingeniería, Universidad de la República, Montevideo, Uruguay, 27 pp., https://iie.fing.edu.uy/publicaciones/2011/Cha11/Chaer%20SimSEE.pdf.

Chin, E. H., 1977: Modelling daily precipitation occurrence process with Markov chain. *Water Resour. Res.*, **13**, 949–956, https://doi.org/10.1029/WR013i006p00949.

Coe, R., and R. D. Stern, 1982: Fitting models to daily rainfall. *J. Appl. Meteor.*, **21**, 1024–1031, https://doi.org/10.1175/1520-0450(1982)021<1024:FMTDRD>2.0.CO;2.

Díaz, A. F., C. D. Studzinski, and C. R. Mechoso, 1998: Relationships between precipitation anomalies in Uruguay and southern Brazil and sea surface temperature in the Pacific and Atlantic Oceans. *J. Climate*, **11**, 251–271, https://doi.org/10.1175/1520-0442(1998)011<0251:RBPAIU>2.0.CO;2.

Gabriel, K. R., and J. Neumann, 1962: A Markov chain model for daily rainfall occurrence at Tel Aviv. *Quart. J. Roy. Meteor. Soc.*, **88**, 90–95, https://doi.org/10.1002/qj.49708837511.

Grimm, A., V. R. Barros, and M. E. Doyle, 2000: Climate variability in southern South America associated with El Niño and La Niña events. *J. Climate*, **13**, 35–58, https://doi.org/10.1175/1520-0442(2000)013<0035:CVISSA>2.0.CO;2.

Grondona, M., G. Podestá, M. Bidegain, M. Marino, and H. Hordij, 2000: A stochastic precipitation generator conditioned on ENSO phase: A case study in southeastern South America. *J. Climate*, **13**, 2973–2986, https://doi.org/10.1175/1520-0442(2000)013<2973:ASPGCO>2.0.CO;2.

Guo, Y., J. Li, and Y. Li, 2014: Seasonal forecasting of north China summer rainfall using a statistical downscaling model. *J. Appl. Meteor. Climatol.*, **53**, 1739–1749, https://doi.org/10.1175/JAMC-D-13-0207.1.

Hansen, J. W., and A. V. M. Ines, 2005: Stochastic disaggregation of monthly rainfall data for crop simulation studies. *Agric. For. Meteor.*, **131**, 233–246, https://doi.org/10.1016/j.agrformet.2005.06.006.

Katz, R. W., 1977a: An application of chain-dependent processes to meteorology. *J. Appl. Probab.*, **14**, 598–603, https://doi.org/10.2307/3213463.

——, 1977b: Precipitation as a chain-dependent process. *J. Appl. Meteor.*, **16**, 671–676, https://doi.org/10.1175/1520-0450(1977)016<0671:PAACDP>2.0.CO;2.

——, and M. B. Parlange, 1996: Mixtures of stochastic processes: Application to statistical downscaling. *Climate Res.*, **7**, 185–193, https://doi.org/10.3354/cr007185.

——, and ——, 1998: Overdispersion phenomenon in stochastic modeling of precipitation. *J. Climate*, **11**, 591–601, https://doi.org/10.1175/1520-0442(1998)011<0591:OPISMO>2.0.CO;2.

Kim, Y., B. Rajagopalan, and G. Lee, 2016: Temporal statistical downscaling of precipitation and temperature forecasts using a stochastic weather generator. *Adv. Atmos. Sci.*, **33**, 175–183, https://doi.org/10.1007/s00376-015-5115-6.

Maciel, F., R. Terra, and R. Chaer, 2015: Economic impact of considering El Niño–Southern Oscillation on the representation of streamflow in an electric system simulator. *Int. J. Climatol.*, **35**, 4094–4102, https://doi.org/10.1002/joc.4269.

Montecinos, A., A. Díaz, and P. Aceituno, 2000: Seasonal diagnostic and predictability of rainfall in subtropical South America based on tropical Pacific SST. *J. Climate*, **13**, 746–758, https://doi.org/10.1175/1520-0442(2000)013<0746:SDAPOR>2.0.CO;2.

Nicholas, R. E., and D. S. Battisti, 2012: Empirical downscaling of high-resolution regional precipitation from large-scale reanalysis fields. *J. Appl. Meteor. Climatol.*, **51**, 100–114, https://doi.org/10.1175/JAMC-D-11-04.1.

Pisciottano, G., A. Díaz, G. Cazes, and C. R. Mechoso, 1994: El Niño–Southern Oscillation impact on rainfall in Uruguay. *J. Climate*, **7**, 1286–1302, https://doi.org/10.1175/1520-0442(1994)007<1286:ENSOIO>2.0.CO;2.

Rajagopalan, B., and U. Lall, 1999: A k-nearest neighbor simulator for daily precipitation and other weather variables. *Water Resour. Res.*, **35**, 3089–3101, https://doi.org/10.1029/1999WR900028.

——, ——, and D. G. Tarboton, 1996: Nonhomogeneous Markov model for daily precipitation. *J. Hydrol. Eng.*, **1**, 33–40, https://doi.org/10.1061/(ASCE)1084-0699(1996)1:1(33).

Racsko, P., L. Szeidl, and M. Semenov, 1991: A serial approach to local stochastic weather models. *Ecol. Modell.*, **57**, 27–41, https://doi.org/10.1016/0304-3800(91)90053-4.

Richardson, C. W., 1981: Stochastic simulation of daily precipitation, temperature and solar radiation. *Water Resour. Res.*, **17**, 182–190, https://doi.org/10.1029/WR017i001p00182.

Ropelewski, C. F., and M. S. Halpert, 1987: Global and regional scale precipitation patterns associated with the El Nino/Southern Oscillation. *Mon. Wea. Rev.*, **115**, 1606–1626, https://doi.org/10.1175/1520-0493(1987)115<1606:GARSPP>2.0.CO;2.

——, and ——, 1989: Precipitation patterns associated with the high index phase of the Southern Oscillation. *J. Climate*, **2**, 268–284, https://doi.org/10.1175/1520-0442(1989)002<0268:PPAWTH>2.0.CO;2.

Semenov, M. A., and E. M. Barrow, 1997: Use of stochastic weather generator in the development of climate change scenarios. *Climatic Change*, **35**, 397–414, https://doi.org/10.1023/A:1005342632279.

Stern, R. D., and R. Coe, 1984: A model fitting analysis of daily rainfall data. *J. Roy. Stat. Soc.*, **147A**, 1–34, https://doi.org/10.2307/2981736.

Trenberth, K. E., 1997: The definition of El Niño. *Bull. Amer. Meteor. Soc.*, **78**, 2771–2777, https://doi.org/10.1175/1520-0477(1997)078<2771:TDOENO>2.0.CO;2.

Verdin, A., B. Rajagopalan, W. Kleiber, G. Podestá, and F. Bert, 2018: A conditional stochastic weather generator for seasonal to multi-decadal simulations. *J. Hydrol.*, **556**, 835–846, https://doi.org/10.1016/j.jhydrol.2015.12.036.

Wilby, R. L., D. Conway, and P. D. Jones, 2002: Prospects for downscaling seasonal precipitation variability using conditioned weather generator parameters. *Hydrol. Processes*, **16**, 1215–1234, https://doi.org/10.1002/hyp.1058.

Wilks, D. S., 1992: Adapting stochastic weather generation algorithms for climate changes studies. *Climatic Change*, **22**, 67–84, https://doi.org/10.1007/BF00143344.

——, 1998: Multisite generalization of a daily stochastic precipitation generation model. *J. Hydrol.*, **210**, 178–191, https://doi.org/10.1016/S0022-1694(98)00186-3.

——, 1999: Interannual variability and extreme-value characteristics of several stochastic daily precipitation models. *Agric. For. Meteor.*, **93**, 153–169, https://doi.org/10.1016/S0168-1923(98)00125-7.

——, 2010: Use of stochastic weather generators for precipitation downscaling. *Wiley Interdiscip. Rev.: Climate Change*, **1**, 898–907, https://doi.org/10.1002/wcc.85.

——, and R. L. Wilby, 1999: The weather generation game: A review of stochastic weather models. *Prog. Phys. Geogr.*, **23**, 329–357, https://doi.org/10.1177/030913339902300302.